

T. Murugan · S. De

# Numerical visualization of counter rotating vortex ring formation ahead of shock tube generated vortex ring

Received: 21 June 2011 / Revised: 29 August 2011 / Accepted: 7 September 2011 / Published online: 11 October 2011  
© The Visualization Society of Japan 2011

**Keywords** Compressible vortex ring · Shock tube · Computational fluid dynamics · Starting jet

## 1 Introduction

Formation of counter rotating vortex ring (CRVR) at the open end of a shock tube at high-shock Mach numbers ( $M$ ) is a fascinating phenomenon. Explanations for CRVR formation that employ qualitative visualization exist in literature. The phenomenon, however, does not seem to be clearly understood. Brouillette and Hebert (1997) first observed the CRVR formation for  $M > 1.6$  using a shadowgraph system. The authors proposed that the CRVR formation was due to flow separation caused by the adverse pressure gradient across the embedded shock. Kontis et al. (2006) observed the formation of multiple CRVR with longer driver section length (DRL) shock tube (750 mm) using schlieren photography for  $M = 1.63$ . They suggested that the generation of these vortex rings depends on the compressibility of the main vortex. Murugan and Das (2009) first observed the complete evolution of CRVR using smoke flow visualization for  $M = 1.7$  with  $DRL = 165$  mm. After formation, the CRVR rolled over the periphery of the primary vortex and ultimately interacted with the trailing jet. Murugan and Das (2010) explained the mechanism of CRVR formation using flow visualization through unsteady changes in the smoke profile. Variable embedded shock strength in the radial direction was thought to be the reason behind the appearance of a shear layer from the triple point of the embedded shock which subsequently rolled-up and formed the CRVR. The exact mechanism responsible for the shear layer roll-up is not clearly understood due to lack of quantitative data such as the strength of the embedded shock, shock cell structure and the vorticity field. Though Ishii et al. (1999) have reported the shock cell structure evolution for a long DRL shock tube (400 mm), quantitative data for unsteady evolution of starting jet for short DRL shock tube (165 mm), which could explain the exact mechanism of CRVR formation better due to less interference from the trailing jet, is not available in literature. In the present study, the mechanism of CRVR formation is identified by solving the axisymmetric Navier–Stokes equations in non-dimensional form using the AUSM+ scheme (Liou 1996). The use of numerical technique allows us to generate the quantitative data, particularly the vorticity field, necessary for clear visualization of this interesting phenomenon.

---

T. Murugan (✉) · S. De  
CSIR, Central Mechanical Engineering Research Institute, Durgapur 713209, West Bengal, India  
E-mail: t\_murugan@cmeri.res.in  
Tel.: +91-343-6452158; +91-343-6452093  
Fax: +91-343-2546745

S. De  
E-mail: s\_de@cmeri.res.in

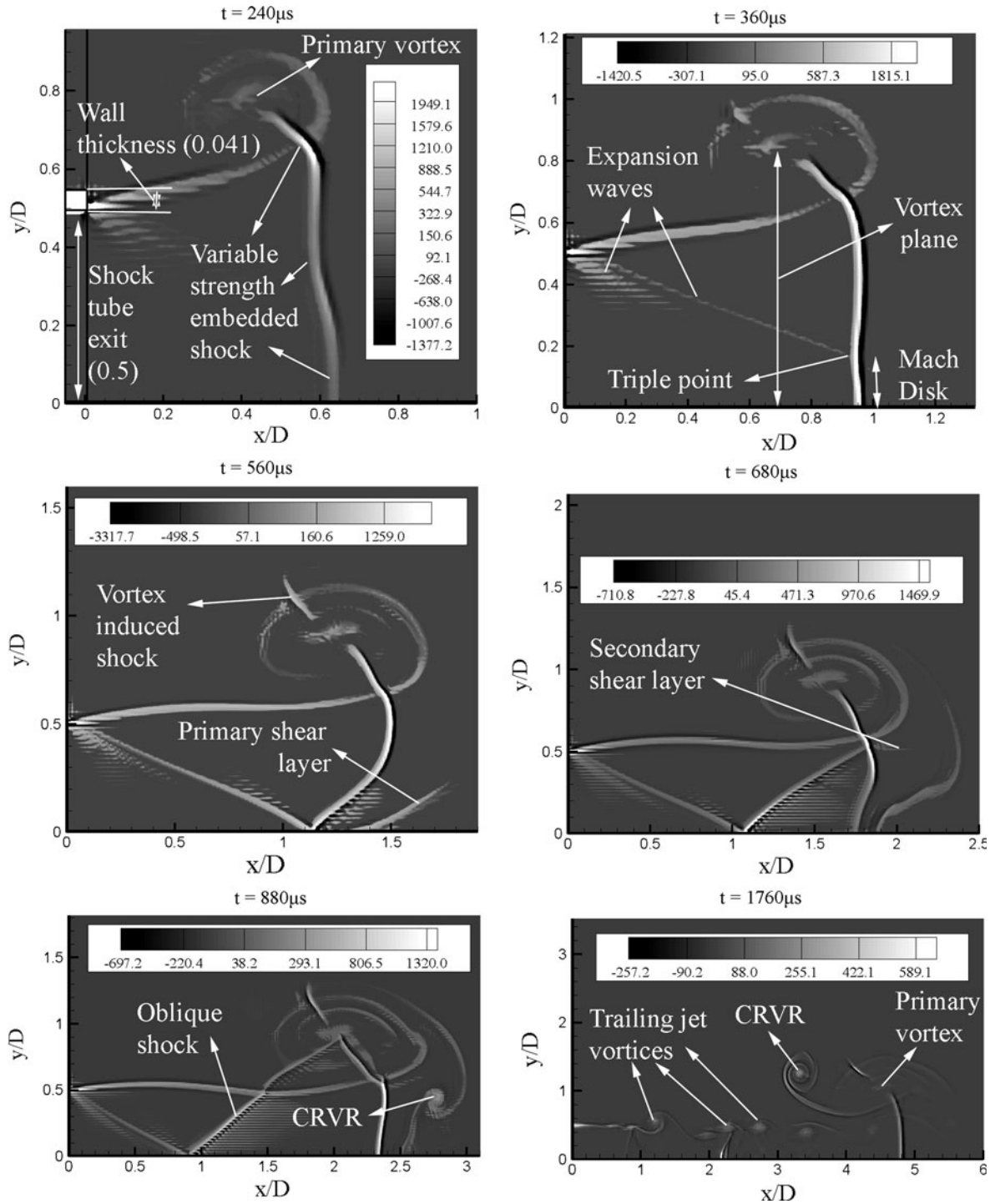


**Fig. 1** Numerical shadowgraph of the starting jet

## 2 Numerical scheme, initial and boundary condition

A shock tube of DRL = 165 mm and driven section length = 1,200 mm is used in the present simulation (Murugan and Das 2010). The inner diameter of the shock tube is 64 mm. The thickness of the shock tube is 2.6 mm. Air is used as the working fluid. The developed axisymmetric Navier–Stokes solver is explicit and convective terms are calculated using the AUSM+ flux vector splitting scheme coupled with second-order

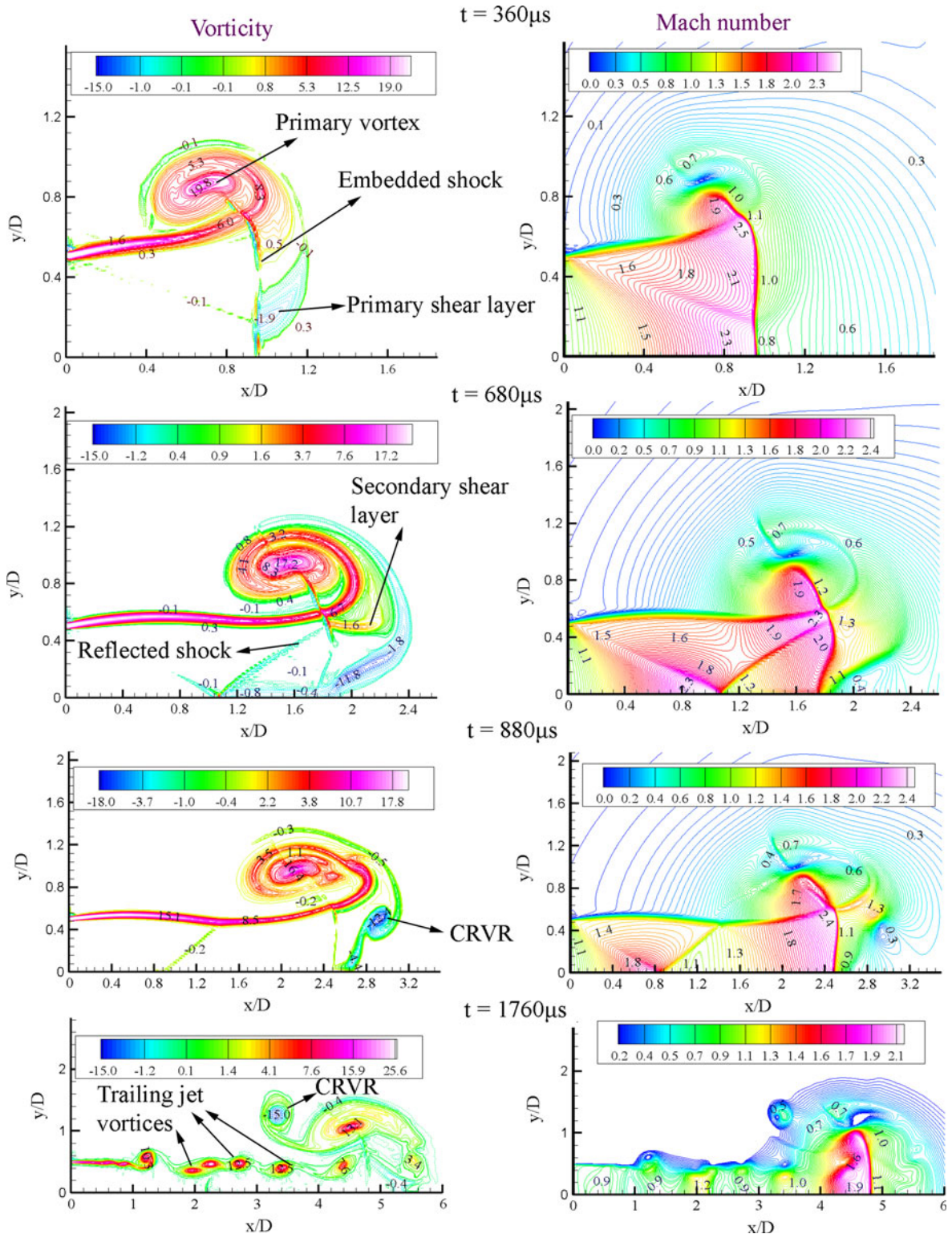


**Fig. 2** Mechanism of counter rotating vortex ring formation

accurate MUSCL extrapolation for computing the primitive variables at the cell faces (De and Murugan 2011). Time stepping is performed using a four-stage Runge–Kutta time integration scheme (Arnone et al. 1993). Viscous fluxes are calculated by standard second-order accurate central differencing formulae. The

driver section is initialized to 10 times the ambient pressure. In the driven section and elsewhere, pressure and temperature are kept at 1.01325 bar and 300 K, respectively. No-slip boundary condition is applied at the tube walls. The centerline is a line of symmetry and NSCBC boundary condition (Poinsot and Lele 1992) is used for computing the flow variables at the open boundaries. The numerical methodology of the solver has been validated for supersonic flow over a  $90^\circ$  bend and a wedge (Schardin's problem). The grid has been kept dense close to the shock tube exit. There are 400 cells in the axial direction over a length of four tube diameters immediately after the tube exit. In the radial direction, 49 cells are uniformly spaced over the tube radius. The grid is progressively coarsened away from the tube exit region in both the directions.

### 3 Results and discussion

Figure 1 shows the numerical shadowgraph of the starting jet. Pressure and  $M$  are 2.95 bar and 0.69, respectively behind the incident shock when it reaches the tube exit ( $x/D = 0$ ). At the open end of the shock tube, the shock diffracts and the flow gradually expands from the outer edge. Flow ahead of the vortex plane in Fig. 1 accelerates due to increase in area ratio and the recirculating flow of vortex. A shock forms within the vortex due to over-expansion and gradually extends up to the axis during vortex ring translation. A Mach disk appears in the axial region at  $t = 360 \mu\text{s}$  as the pressure ratio is greater than 2 (Ishii et al. 1999) at the lip after the flow reaches sonic condition. Figure 2 shows the vorticity and Mach contours of the starting jet. A shear layer (primary) forms at the triple point due to velocity gradient at  $t = 360 \mu\text{s}$  and its negative vorticity is entrained by the primary vortex. No CRVR is noticed at this point. As the main vortex drifts downstream, the triple point moves towards the axis and a reflected shock forms that ends on the embedded shock, leading to another triple point ( $t = 680 \mu\text{s}$ ). This second triple point gives rise to the secondary shear layer with positive vorticity, which pulls the primary shear layer underneath. This leads to the roll-up of the CRVR, clearly visible at  $t = 840 \mu\text{s}$ . The results presented here do not include effects of turbulence models and three-dimensionality. These will be investigated in future.

### References

- Arnone A, Liou MS, Povinelli LA (1993) Multigrid time-accurate integration of Navier–Stokes equations. NASA TM 106373
- Brouillette M, Hebert C (1997) Propagation and interaction of shock-generated vortices. *Fluid Dyn Res* 21:159–169
- De S, Murugan T (2011) Numerical simulation of shock tube generated vortex: effect of numerics. *Int J Comp Fluid Dyn* 25:345–354
- Ishii R, Fujimoto H, Hatta N, Umeda Y (1999) Experimental and numerical analysis of circular pulse jets. *J Fluid Mech* 392:129–153
- Kontis K, An R, Edwards JA (2006) Compressible vortex-ring studies with a number of generic body configurations. *AIAA* 44:2962–2978
- Liou M-S (1996) A sequel to AUSM: AUSM+. *J Comput Phys* 129:364–382
- Murugan T, Das D (2009) On the evolution of counter rotating vortex formed ahead of a compressible vortex ring. *J Vis* 12:3
- Murugan T, Das D (2010) Characteristics of counter-rotating vortex rings formed ahead of a compressible vortex ring. *Exp Fluids* 49:1247–1261
- Poinsot TJ, Lele SK (1992) Boundary conditions for direct simulations of compressible viscous flows. *J Comput Phys* 101:104–129